J Indian Soc Remote Sens (February 2018) 46(2):211–218
https://doi.org/10.1007/s12524-017-0690-x

RESEARCH ARTICLE

Surface Reflectance Climate Data Records (CDRs) is a Reliable Landsat ETM+ Source to Study Chlorophyll Content in Pecan Orchards

Yahia Othman[1,2] · Caiti Steele[3] · Rolston St. Hilaire[1]

Received: 6 December 2016 / Accepted: 30 April 2017 / Published online: 20 June 2017

Abstract We evaluated the relationships among three Landsat Enhanced Thematic Mapper (ETM+) datasets, top-of-atmosphere (TOA) reflectance, surface reflectance climate data records (surface reflectance-$_{CDR}$) and atmospherically corrected images using Fast Line-of-Sight atmospheric analysis of Spectral Hypercubes model (surface reflectance-$_{FLAASH}$) and their linkto pecan foliar chlorophyll content(chl-cont). Foliar chlorophyll content as determined with a SPAD meter, and remotely-sensed data were collected from two mature pecan orchards (one grown in a sandy loam and the other in clay loam soil) during the experimental period. Enhanced vegetation index derived from remotely sensed data was correlated to chl-cont. At both orchards, TOA reflectance was significantly lower than surface reflectance within the 550–2400 nm wavelength range. Reflectance from atmospherically corrected images (surface reflectance-$_{CDR}$ and surface reflectance-$_{FLAASH}$) was similar in the shortwave infrared (SWIR: 1550–1750 and 2080–2350 nm) and statistically different in the visible (350–700 nm). Enhanced vegetation index derived from surface reflectance-$_{CDR}$ and surface reflectance-$_{FLAASH}$ had higher correlation with chl-cont than TOA. Accordingly, surface reflectance is an essential prerequisite for using Landsat ETM+ data and TOA reflectance could lead to miss-/or underestimate chl-cont in pecan orchards. Interestingly, the correlation comparisons (Williams *t* test) between surface reflectance-$_{CDR}$ and chl-cont was statistically similar to the correlation between chl-cont and commercial atmospheric correction model. Overall, surface reflectance-$_{CDR}$, which is freely available from the earth explorer portal, is a reliable atmospherically corrected Landsat ETM+ image source to study foliar chlorophyll content in pecan orchards.

Keywords Landsat · Chlorophyll content · Remote sensing · *Carya illinoinensis*

Introduction

Volatility in the cost of agricultural inputs and outcomes causes instability in farm profits. This instability mandates the introduction of new farming approaches such as, precision agriculture to stabilize the farm economy. Precision agriculture supports field management practices based on modern technologies such as yield monitoring instrumentation, geographic information systems and remote sensing (Seelan et al. 2003).

The use of remote sensing in precision agriculture is not new (Othman et al. 2014; Xiao et al. 2005). For example, Othman et al. (2014) found that surface reflectance data derived from Landsat sensors holds promise for detecting water deficit in pecan (*Carya illinoinensis*) orchards. However, inadequate repeated measurements during the growing season, coarse spatial and spectral resolution and atmosphric attentution couldlimit the overall utility of space-borne remote sensing data (Chander et al. 2009; Moran et al. 1997; Primicerio et al. 2012).

The atmosphere reduces reflected light from the canopy and this diminishes reflectance significantly. This lessened

✉ Rolston St. Hilaire
rsthilai@nmsu.edu

[1] Plant and Environmental Sciences, New Mexico State University, Las Cruces, NM, USA

[2] Department of Horticulture and Crop Science, University of Jordan, Amman, Jordan

[3] Jornada Experimental Range, New Mexico State University, ARS–USDA, Las Cruces, NM, USA

reflectance reduces the performance of remote sensing systems (Jensen 2005). However, atmospheric attenuation may not be a significant issue for specific remote sensing applications. For example, correcting Landsat TM images for atmosphere is unnecessary in image classification studies, but mandatory for those that monitor terrestrial areas over time (Song et al. 2001).

Algorithms such as, FLAASH, CDRs and dark object subtraction have been used to reduce the atmospheric attenuation in satellite sensor data (Butson and Fernandes 2004; Cooley et al. 2002; Othman et al. 2014). FLAASH is a commercial model and derives its physics-base from the MODTRAN4 radiative transfer algorithm. This model potentially improved the accuracy of remotely-sensed data by providing precise and physics-base derivation of aerosol, water vapor column, surface pressure and cloud overburdens (Cooley et al. 2002). However, atmospheric correction models require data related to the condition of the atmosphere at the time the image is acquired (Chrysoulakis et al. 2010). Collecting atmospheric data is time consuming, expensive, and not always possible (Chrysoulakis et al. 2010). The conversion of at-sensor spectral radiance to TOA can also be used to reduce image-to-image variability over time (Chander et al. 2009). However, TOA reflectance does not account for atmospheric effects, which can be significant (Chavez 1996) and variable during the growing season.

High spatial and spectral sensors such as RapidEye, Sentinel-2, and handheld spectroradiometer potentially detect crop growth, physiology and development during the growing season (Kross et al. 2015; Othman et al. 2015). However, input cost could be a drawback to farmer adoption. Landsat sensor data hold promise for detecting pecan physiological status (Othman et al. 2014). The commercial FLAASH atmospheric algorithm has been used to process Landsat sensors images to study pecan physiology (Othman et al. 2014). But, FLAASH requires ground data at the time the image is acquired and licensing costs. Landsat ETM+ TOA and atmospherically corrected images (surface reflectance$_{\text{-CDR}}$) are freely available from the earth-explorer portal. However, the reliability of those Landsat datasets to assess chl-cont in pecan is not known.

Measuring foliar chl-cont is important because it is associated with abiotic stresses (Huang et al. 2015) and yield (Ramírez et al. 2014), can be used as a proxy for nitrogen status in trees including pecans (Hardin et al. 2012), and is a rapid and easy nondestructive measurement to assess the health of trees (Percival et al. 2008). However, collecting physiological measurements from pecan trees which can grow to 30 m is quite challenging. Using remotely-sensed data from Landsat ETM+ to detect chl-cont could speed and scale up the measurements to large areas. But, estimating chl-cont from space is influenced by atmospheric conditions and background reflectance (Daughtry et al. 2000). Accordingly, finding reliable Landsat ETM+ dataset to study foliar chlorophyll content in pecan can be of great interest. The objective of this study was to evaluate the usefulness of Landsat ETM+ TOA reflectance, atmospherically corrected images from earth-explorer NASA data portal (surface reflectance-$_{\text{CDR}}$) and atmospherically corrected data set using FLAASH model (surface reflectance-$_{\text{FLAASH}}$) for detecting pecan chl-cont.

Materials and Methods

Study Sites

This study was carried out in two seasons, from May 25, 2012 to Nov. 20, 2013 over two mature pecan (*Carya illinoinensis* Wangenh. C. Koch) orchards in the Mesilla Valley, New Mexico, USA. Pecan is the major orchard crop in this area. Site 1 was located in the northern Mesilla Valley (32°17′06.25″N, 106°50′04.26″ W, elevation 1185 m) and site 2 was at New Mexico State University's Leyendecker Plant Science Research Center (32°12′ 01.14″ N, 106°44′30.32″ W, elevation 1173 m). Trees from site 1 were about 30 years old, 7–10 m wide (canopy), 9–11 m high, grown in sandy loam soil, and spaced at 6–7 m within rows and 8–10 m between rows. The orchard was flood-irrigated once every 16–24 days from May to October every year. Site 2 trees were 20–30 years old, 4–6 m wide (canopy), 7–9 m high, grown in clay loam soil, spaced at 6–7 m within rows and 8 m between rows and flood-irrigated once every 3–10 weeks from May to November every year.

Ground Reference Sampling

Ten trees were selected randomly from both sites for chl-cont and handheld spectroradiometer hyperspectral measurements (Table 1). Measurements were taken between 11:00 a.m. and 1:00 p.m. Leaf chl-cont was determined using a chlorophyll meter (SPAD-502 Plus, Minolta, Japan). SPAD readings were converted to chlorophyll content using the equation of Percival et al. (2008).

$$\text{Total chl - cont } (\mu g/\text{g FW}) = 1.8159 \times \text{SPAD}^{0.8809} \quad (1)$$

Field measurements were synchronized with the overpasses of the Landsat 7 ETM+ satellite acquisition dates.

Remotely-Sensed Data Acquisition and Analysis

We used three Landsat ETM+ datasets; TOA, surface reflectance$_{\text{-CDR}}$ and surface reflectance$_{\text{-FLAASH}}$. Field-level reflectance from the handheld spectroradiometer (ASD,

Table 1 Handheld spectroradiometer and chlorophyll content (SPAD) measurements and Landsat ETM+ acquisition dates for both sites during the 2012 and 2013 experimental period

Site	Year	Date of Measurement
Site 1 (sandy loam)	2012	26 May, 11 June, 27 June, 13 August, 15 September, 1 October, 17 October
	2013	29 May, 2 September, 18 September, 4 October
Site 2 (clay loam)	2012	26 May, 11 June, 27 June, 30 August, 15 September, 17 October, 2 November
	2013	29 May, 14 June, 17 August, 2 September, 20 October

Fieldspec Pro 2, Analytical Spectral Devices, Boulder, CO, USA) was also used to assess the impact of soil background and atmosphere on the correlation between remotely sensed data and chl-cont. Cloud free Landsat 7 ETM+ Imagery was identified and downloaded from United States Geological Survey Global Visualization Viewer (USGS 2015a). Images then were georectified with 1 m orthophotography (NAIP 2011) using Environment for Visualizing Images (ENVI) 5.0 (Research Systems, Boulder, CO, USA). TOA reflectance was derived from the imagery uncalibrated digital numbers using the equation of Irish (1998):

$$\rho_{TOA} = \pi \, L_\lambda d^2 / ESUN_\lambda \cos \theta_s \quad (2)$$

where L_λ is the at-sensor spectral radiance at band λ, d is Sun-Earth distance in astronomical units, $ESUN_\lambda$ is the mean solar irradiance for band λ and θ_s is the solar zenith angle in degrees. For Landsat ETM+ surface reflectance, two data sets were used. The first dataset (surface reflectance$_{-CDR}$) are atmospherically corrected Landsat ETM+ scenes available from the earth-explorer NASA portal (USGS 2015b). Landsat surface.

Reflectance$_{-CDR}$ images are atmospherically corrected using the Landsat Ecosystem Disturbance Adaptive Processing System (LEDAPS) program. During image preprocessing, LEDAPS applies Moderate Resolution Imaging Spectroradiometer atmospheric correction routines to ETM+ Level-1 images (USGS 2015b). The second ETM+ set was derived using FLAASH atmospheric correction algorithm in ENVI.FLAASH incorporates MODTRAN atmosphere models (Matthew et al. 2000). In FLAASH, United States Standard Atmospheric Model was used to determine water vapor concentration and Rural aerosol was the aerosol type. Atmospheric model was selected according to the known weather and initial visibility data collected from Las Cruces airport and the nearby weather stations (<5 km from study sites). For aerosol model, four drop-down list of the standard MODTRAN aerosol/haze types are available (1) tropospheric, applies to calm, clear conditions (visibility >40 km) (2) maritime represents the boundary layer over oceans (3) urban appropriate for high-density urban/industrial areas and (4) rural which represents aerosols in areas not affected by high urban density. Because both sites were located in areas not strongly affected by urban or industrial sources and the visibility was <40 km, the Rural aerosol model was selected.

Field-level reflectance was determined by simulating Landsat ETM+ surface reflectance using handheld spectroradiometer data. Canopy spectral reflectance within the 350–2500 nm spectral range (1 m nadir distance) was first measured on clear sky days between 11:00 a.m. and 1:00 p.m. with the handheld spectroradiometer. Field-level reflectance measurements were synchronized with the overpasses of the Landsat 7 ETM+ satellite acquisition dates. A hydraulic manlift (10-m platform height) was used to raise the operator and the handheld spectroradiometer instrument above the tree canopy (Fig. 1). The

Fig. 1 *Left* field-level surface reflectance measurements using handheld spectroradiometer, and *right* instrument calibration using calibrated diffuse white reference panel

spectroradiometer sensor (25 field of view) was oriented in a nadir position above the canopy. The distance from the top of the canopy and the spectroradiometer sensor was 1 m. An average of ten spectral measurements distributed to cover the top part of the canopy was used (Fig. 1). Then, Landsat ETM+ bands were simulated by convolving the hyperspectral bands with the relative response curves for the visible (VIS) and the NIR bands (USGS 2015c). During convolving process, handheld spectroradiometer bands were convolved with the relative spectral response curves. The spectral response function used in convolving process for blue band (ETM+ band 1) ranged from 410 to 522 nm, green (ETM+ band 2) ranged from 500 to 650, red (ETM+ band 3) ranged from 580 to 740 nm, NIR (ETM+ band 4) ranged from 730 to 945 nm, SWIR (ETM+ band 5) ranged from 1514 to 1880 nm and SWIR (ETM+ band 7) ranged from 2000 to 2400 nm. A weighted average for convolved bands was calculated using the following equation:

$$\text{Weighted average for band } (x) = w_1x_1 + w_2x_2 \ldots w_nx_n \quad (3)$$

where w is relative weight (%) of specific ETM+ band and x is the specific specroradiometer band correspond to the same ETM+ band. Then, the total sum of the hyperspectral bands was calculated to derive the simulated Landsat ETM+ reflectance (field-level reflectance). For Landsat ETM+ data, the total fraction of vegetation cover/soil visible in Landsat ETM+ pixel was about 55–65% in site 1 and 50–55% in site 2. The trees location in the pixel was determined from aerial photographs. Then, the pixel that represented the location of trees was used to derive vegetation indices that significantly detected chlorophyll content in other crops. Vegetation indices included, Enhanced Vegetation Index (Huete et al. 2002), Chlorophyll Index-Green (Gitelson et al. 2003), Triangular Vegetation Index (Broge and Leblanc 2000), Chlorophyll Vegetation Index (Vincini et al. 2008), and Normalized Difference Vegetation Index (Rouse 1974). The EVI was vegetation index that best detected chlorophyll content. For this reason only the EVI results are presented:

$$\text{EVI} = \text{G} \times (\rho_{\text{NIR}} - \rho_{\text{R}})/(\rho_{\text{NIR}} + \text{C}_1 \times \rho_{\text{R}} - \text{C}_2 \times \rho_{\text{B}} + \text{L}) \quad (4)$$

where ρ_{NIR}, ρ_{R} and ρ_{B} are reflectance at NIR red and blue bands from TOA and atmospherically corrected images; C1 and C2 are the coefficients of aerosol resistance (C1 = 6 and C2 = 7.5), G is the gain factor (G = 2.5), and L is the canopy background adjustment (L = 1). The coefficients C_1 and C_2, G, and L used in the EVI equation were adopted from Huete et al. (1994, 1997).

Statistical Analysis

Analysis of variance and Fisher's least significant difference ($P = 0.05$) were used to compare Landsat ETM+ wavelength reflectance from TOA, surface reflectance$_{\text{-CDR}}$ and surface reflectance$_{\text{-FLAASH}}$. Due to the fact that field-level reflectance (using handheld spectroradiometer) and Landsat ETM+ datasets (TOA, CDR, and FLAASH) represent different land surface and are not comparable, field-level reflectance did not include in mean separation analysis (Fig. 2). Pearson correlation was conducted to assess the relationship between chl-cont and remotely sensed data. Then, Williams's *t*-test was used to compare Pearson correlations coefficients (Williams 1959). We used the *t* test to determine if the atmospheric correction of Landsat ETM+ data significantly improved the correlation between remotely sensed data and chl-cont. In William's *t* test, two non-independent correlations with a variable in common (chl-cont) as described by Weaver and Wuensch (2013) were used.

Results and Discussions

Mean separation revealed significant differences in reflectance between TOA and atmospherically corrected images across the wavelengths and over both sites (Fig. 2). Except for blue band (450–520 nm), TOA (Fig. 2a, b) had lower reflectance than Landsat ETM+ surface reflectance$_{\text{-FLAASH}}$ (Fig. 2c, d) and surface reflectance$_{\text{-CDR}}$ (Fig. 2e, f) at both sites and across sampling dates (2012 and 2013). These results conflict with the spectral properties of plants which normally reflect more light in the green than the blue spectral regions (Gates et al. 1965). However, this is normal for non-atmospherically corrected data. Within the visible and NIR spectral range, a significant difference in reflectance was found between surface reflectance$_{\text{-FLAASH}}$ (Fig. 2c, d) and surface reflectance$_{\text{-CDR}}$ (Fig. 2e, f). But, no significant difference was found between atmospherically images in the SWIR (1550–1750 and 2080–2350 nm) spectrum regions.

Field-level reflectance had higher canopy surface reflectance in VIS (350–700 nm), NIR (700–1200 nm), and SWIR bands than the TOA and surface reflectance at both sites (Figs. 2a, b). Lower reflectance within the NIR and SWIR in both TOA and surface reflectance data could be attributed to atmospheric absorption (Jensen 2005). Furthermore, the pixel size of ETM+ is 30 by 30 m and this pixel contains trees and soils. In contrast, field-level reflectance data from handheld spectroradiometer (1 m above canopy) has limited soil background reflectance in the pixel. Because ETM + data sets contains mixed pixels

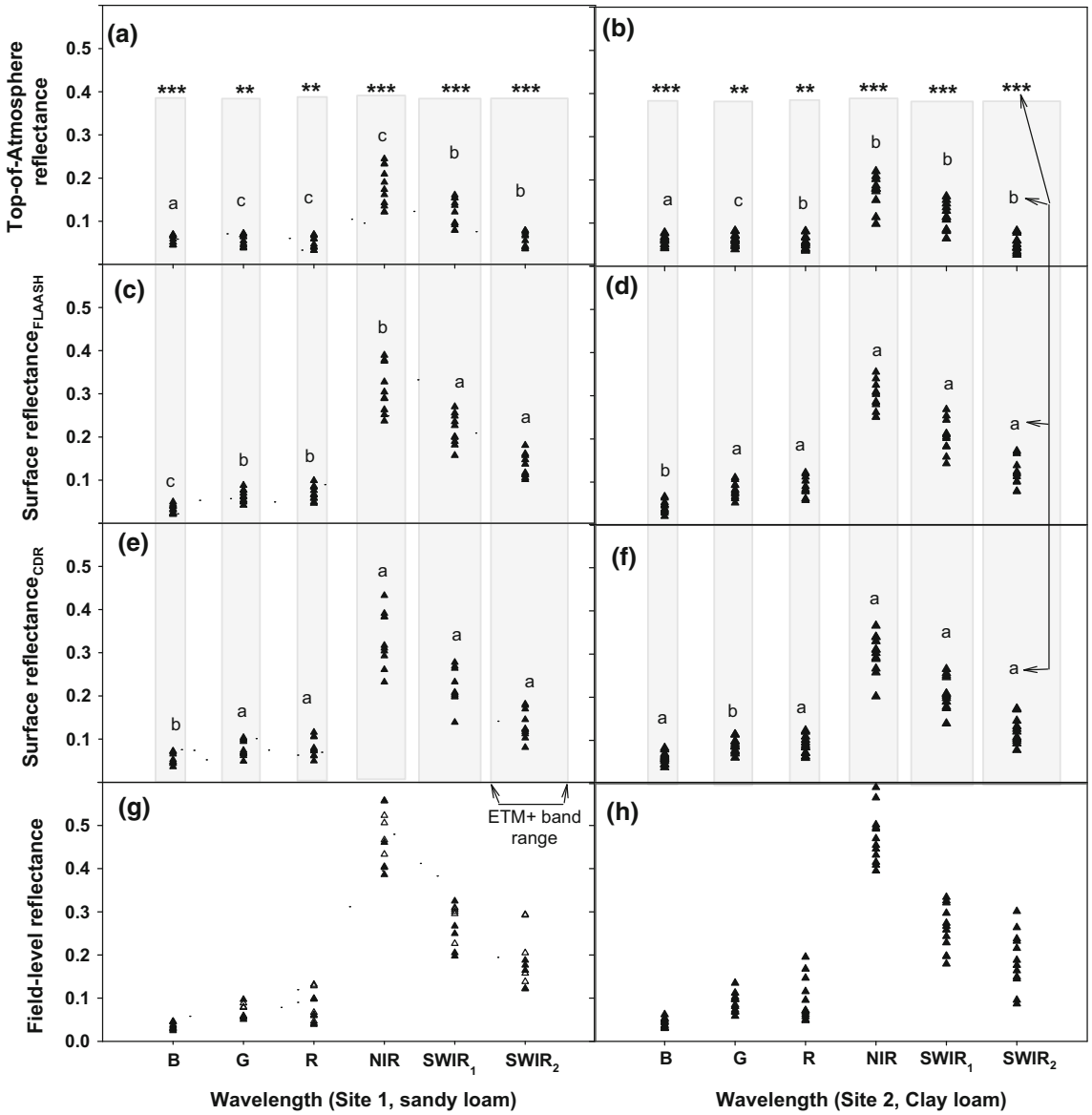

Fig. 2 Wavelengths reflectance derived from Landsat ETM+ (**a**, **b**) top-of-atmosphere (**c**, **d**) surface reflectance$_{\text{FLAASH}}$ (**e**, **f**) surface reflectance$_{\text{CDR}}$ and (**g**, **h**) field-level reflectance at site 1 (sandy loam soil) and site 2 (clay loam soil) during the study period 2012 and 2013. Orchards are located in the Mesilla Valley, New Mexico. At each wavelength, mean with different letters are significantly difference across the datasets at $P = 0.05$.*Double asterisk* and *triple asterisk* denote significance at $P < 0.01$, and $P < 0.001$, respectively. Because field-level reflectance and Landsat ETM+ represent different land surface, field-level reflectance did not included in the mean separation analysis

of vegetation and soil which make the two datasets incomparable, field-level reflectance was not included in the mean separation process (Fig. 2).

Enhanced vegetation index was developed using partially or fully corrected atmospheric corrected reflectance data in order to optimize the vegetation signal in high biomass regions (Huete et al. 2002). In our study, TOA reflectance data which did not account for atmospheric effects was also used to derive EVI. This is because the accuracy of atmospheric correction models are variable (López-Serrano et al. 2016) and could be low. Additionally, direct use of measured TOA reflectance has been recommended for estimating biophysical and biochemical variable in forests studies (Laurent et al. 2011). Tebbs et al. (2013) found that near infrared (NIR): red (R) ratio derived from Landsat TOA reflectance gave a better fit to chlorophyll-a than atmospherically corrected data. However, EVI derived from TOA had the lowest correlation with chl-cont when compared to surface reflectance datasets (Fig. 3). The correlation coefficient was 0.22in site 1 (Fig. 3a) and 0.5 in site 2 (Fig. 3b). Williams's *t*-test matrix (Table 2) revealed that

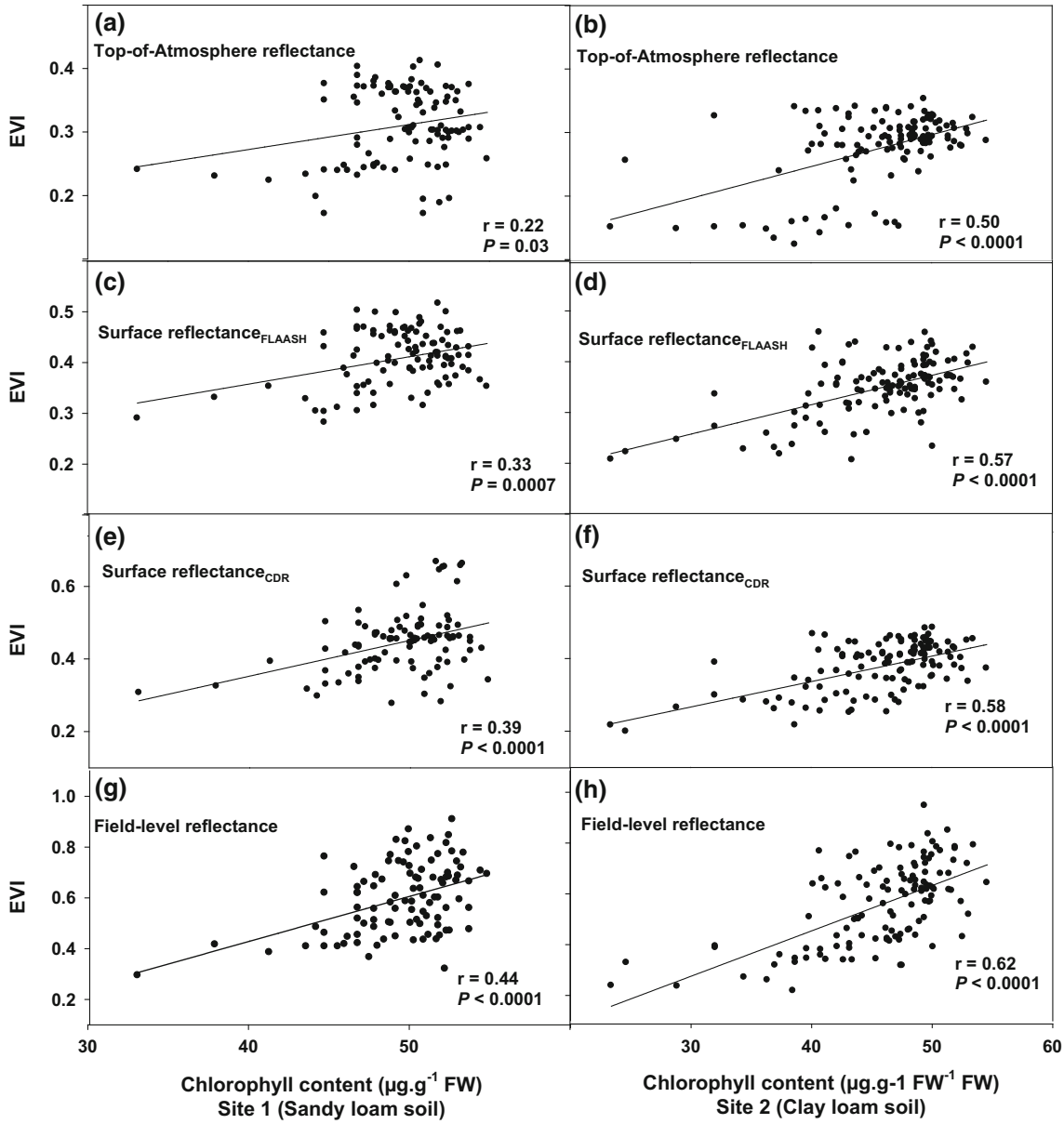

Fig. 3 Correlation coefficients between chlorophyll content (µg g^{-1} fresh weight) and enhanced vegetation index (EVI) from Landsat ETM + (**a**, **b**) top-of-atmosphere (**c**, **d**) surface reflectance$_{\text{-FLAASH}}$ (**e**, **f**) surface reflectance$_{\text{-CDR}}$ and (**g**, **h**) field-level reflectance at both sites during the experimental period, 2012 and 2013. Orchards are located in the Mesilla Valley, New Mexico

atmospheric correction process significantly improved the correlation between Landsat ETM + data and chl-cont when compared to non-processed images (TOA in site 1). In fact, the correlation coefficients from atmospherically corrected images (surface reflectance$_{\text{-CDR}}$ and surface reflectance$_{\text{-FLAASH}}$) were statistically similar to those from field-level reflectance (limited soil background and atmosphere effect) (Table 2). Interestingly, Williams's *t*-test revealed that EVI-surface reflectance$_{\text{-CDR}}$ which is freely available from the earth-explorer was statistically similar to surface reflectance derived using the commercial atmospheric model, FLAASH. Overall, atmospherically corrected scene (surface reflectance$_{\text{-CDR}}$) available from the earth-explorer significantly improved the capability of Landsat ETM+ to detect chl-cont in pecan and was similar to those corrected using commercial atmospheric algorithm (surface reflectance$_{\text{-FLAASH}}$).

Conclusions

At both orchards, TOA reflectance was significantly lower than surface reflectance within NIR and SWIR spectral regions. Additionally, the correlation between TOA-EVI

Table 2 Correlation comparisons matrix (Williams' test) for enhanced vegetation index derived from Landsat ETM + surface reflectance (FLAASH and CDR), Landsat ETM + top-of-atmosphere (TOA) and field-level reflectance (ASD) using handheld spectroradiometer at both sites during the study period 2012 and 2013

Location	Correlation Comparison	*t* test	*P* value
	Landsat ETM+ TOA and surface reflectance		
Site 1 (sandy loam)	FLAASH vs. CDR	−0.21	0.510
	FLAASH vs. TOA	1.99	0.048
	CDR vs. TOA	2.01	0.047
Site 2 (clay loam)	FLAASH vs. CDR	−0.21	0.840
	FLAASH vs. TOA	0.97	0.350
	CDR vs. TOA	1.45	0.150
	Landsat ETM+ and Field-level reflectance		
Site 1 (sandy loam)	FLAASH vs. ASD	−1.17	0.250
	CDR vs. ASD	−0.55	0.59
	TOA vs. ASD	−2.47	0.015
Site 2 (clay loam)	FLAASH vs. ASD	−0.94	0.350
	CDR vs. ASD	-0.74	0.450
	TOA vs. ASD	-1.82	0.07

Orchards (sites 1 and 2) are located in the Mesilla Valley, New Mexico. Sample size n = 110 at site 1 and 120 at site 2

was significantly lower than surface reflectance in sandy loam site. Therefore, surface reflectance is essential in detecting chl-cont in pecan trees. However, EVI derived using commercial atmospheric algorithm (FLAASH) was similar to surface reflectance data available from earth-explorer portal. Accordingly, using Landsat ETM + surface reflectance-$_{CDR}$ is sufficient and reliable atmospheric corrected image source to study foliar chlorophyll content in pecan orchards.

References

Broge, N., & Leblanc, E. (2000). Comparing predictive power and stability of broadband and hyperspectral vegetation indices for estimation of green leaf area index and canopy chlorophyll density. *Remote Sensing of Environment, 76,* 156–172.

Butson, C., & Fernandes, R. (2004). A consistency analysis of surface reflectance and leaf area index retrieval from overlapping clear-sky Landsat ETM+ imagery. *Remote Sensing of Environment, 89,* 369–380.

Chander, G., Markham, B., & Helder, D. (2009). Summary of current radiometric calibration coefficients for Landsat MSS, TM, ETM + , and EO-1 ALI sensors. *Remote Sensing of Environment, 113,* 893–903.

Chavez, P. (1996). Image-based atmospheric corrections revisited and improved. *Photogrammetric Engineering Remote Sensing, 62,* 1025–1036.

Chrysoulakis, N., Abrams, M., Feidas, H., & Arai, K. (2010). Comparison of atmospheric correction methods using ASTER data for the area of Crete, Greece. *International Journal of Remote Sensing, 31,* 6347–6385.

Cooley, T., Anderson, G., Felde, M., Hoke, A., Ratkowskia, H., Chetwynd, J., et al. (2002). FLAASH, a MODTRAN4-based atmospheric correction algorithm, its application and validation. *Geoscience and Remote Sensing Symposium, 3,* 1414–1418.

Daughtry, C., Walthall, C., Kim, M., Colstoun, E., & McMurtrey, J., III. (2000). Estimating corn leaf chlorophyll concentration from leaf and canopy reflectance. *Remote Sensing of Environment, 74,* 229–239.

Gates, D., Keegan, H., Schleter, J., & Weidner, V. (1965). Spectral properties of plants. *Applied Optics, 4*(1), 11–20.

Gitelson, A., Gritz, Y., & Merzlyak, M. (2003). Relationships between leaf chlorophyll content and spectral reflectance algorithms for non-destructive chlorophyll assessment in higher plants. *Journal of Plant Physiology, 160,* 271–282.

Hardin, J., Smith, M., Weckler, P., & Cheary, B. (2012). In situ measurement of pecan leaf nitrogen concentration using a chlorophyll meter and vis-near infrared multispectral camera. *HortScience, 47*(7), 955–960.

Huang, C., Wei, G., Jie, Y., Xu, J., Zhao, S., Wang, L., et al. (2015). Responses of gas exchange, chlorophyll synthesis and ROS-scavenging systems to salinity stress in two ramie (*Boehmeria nivea* L.) cultivars. *Photosynthetica, 53*(3), 455–463.

Huete, A., Didan, K., Miura, T., Rodriguez, E., Gao, X., & Ferreira, L. (2002). Overview of the radiometric and biophysical performance of the MODIS vegetation indices. *Remote Sensing of Environment, 83,* 195–213.

Huete, A., Justice, C., & Liu, H. (1994). Development of vegetation and soil indices for MODIS-EOS. *Remote Sensing of Environment, 49,* 224–234.

Huete, A., Liu, H. Q., Batchily, K., & van Leeuwen, W. (1997). A comparison of vegetation indices over a global set of TM images for EOS-MODIS. *Remote Sensing of Environment, 59,* 440–451.

Irish, R. (1998). *Landsat 7 science data user's handbook*. Greenbelt: Goddard Space Flight Center.

Jensen, J. (2005). *Introductory digital image processing: A remote sensing perspective*. Upper Saddle River: Prentice Hall.

Kross, K., McNairn, H., Lapen, D., Sunohara, M., & Champagne, C. (2015). Assessment of RapidEye vegetation indices for estimation of leaf area index and biomass in corn and soybean crops. *International Journal of Applied Earth Observation and Geoinformation, 34,* 235–248.

Laurent, V., Verhoef, W., Clevers, J., & Schaepman, M. (2011). Estimating forest variables from top-of-atmosphere radiance satellite measurements using coupled radiative transfer models. *Remote Sensing of Environment, 115,* 1043–1052.

López-Serrano, P., Corral-Rivas, J., Díaz-Varela, R., Álvarez-González, J., & López-Sánchez, C. (2016). Evaluation of radiometric and atmospheric correction algorithms for aboveground forest biomass estimation using Landsat 5^{TM} data. *Remote Sensing, 369,* 1–19.

Matthew, M., Adler-Golden, S., Berk, A., Richtsmeier, S., Levine, R., Bernstein, L., et al. (2000). Status of atmospheric correction using a MODTRAN4-based algorithm.SPIE proceedings. *Algorithms for Multispectral, Hyperspectral, and Ultraspectral Imagery VI, 4049,* 199–207.

Moran, M., Inoue, Y., & Barnes, E. (1997). Opportunities and limitations for image-based remote sensing in precision crop management. *Remote Sensing of Environment, 61,* 319–346.

NAIP. (2011). National agriculture imagery program. http://rgis.unm.edu/#map Accessed December 2, 2016.

Othman, Y., Steele, C., VanLeeuwen, D., Heerema, R., Bawazir, S., & Hilaire, R. S. (2014). Remote sensing used to detect moisture status of pecan orchards grown in a desert environment. *International Journal of Remote Sensing, 35*(3), 949–966.

Othman, Y., Steele, C., VanLeeuwen, D., & Hilaire, R. S. (2015). Hyperspectral surface reflectance data used to detect moisture

status of pecan orchards during flood irrigation. *Journal of the American Society for Horticultural Science, 140*(5), 449–458.

Percival, G., Keary, I., & Noviss, K. (2008). The potential of a chlorophyll content SPAD meter to quantify nutrient stress in foliar tissue of sycamore (*Acer pseudoplatanus*), english oak (*Quercus robur*), and european beech (*Fagus sylvatica*). *Arboriculture & Urban Forestry, 34*(2), 89–100.

Primicerio, J., Di Gennaro, S., Fiorillo, E., Genesio, L., Lugato, E., Matese, A., et al. (2012). A flexible unmanned aerial vehicle for precision agriculture. *Precision Agriculture, 13,* 517–523.

Ramírez, D., Yactayo, W., Gutiérrez, R., Mares, V., & De Mendiburu, F. (2014). Chlorophyll concentration in leaves is an indicator of potato tuber yield in water-shortage conditions. *Scientia Horticulturae, 168,* 202–209.

Rouse, J. (1974). *Monitoring the vernal advancement and retrogradation (green wave effect) of natural vegetation*. http://ntrs.nasa.gov/archive/nasa/casi.ntrs.nasa.gov/19730017588.pdf Accessed December 2, 2016.

Seelan, S., Laguette, S., Casady, G., & Seielstad, G. (2003). Remote sensing applications for precision agriculture: A learning community approach. *Remote Sensing of Environment, 88,* 157–169.

Song, C., Woodcock, C., Seto, K., Lenney, M., & Macomber, S. (2001). Classification and change detection using Landsat TM data: When and how to correct atmospheric effects? *Remote Sensing of Environment, 75,* 230–244.

Tebbs, E., Remedios, J., & Harper, D. (2013). Remote sensing of chlorophyll-a as a measure of cyanobacterial biomass in Lake Bogoria, a hyertrophic, saline-alkaline, flamingo lake, using Landsat ETM+. *Remote Sensing of Environment, 135,* 92–106.

USGS. (2015a). USGS Global visualization viewer. http://glovis.usgs.gov/ Accessed December 2, 2016.

USGS. (2015b). USGS earth explorer. Accessed December 2, 2016.

USGS. (2015c). Landsat satellites relative spectral responses.

Vincini, M., Frazzi, E., & D'Alessio, P. (2008). A broad-band leaf chlorophyll index at the canopy scale. *Precision Agriculture, 9,* 303–319.

Weaver, B., & Wuensch, K. (2013). SPSS and SAS programs for comparing Pearson correlations and OLS regression coefficients. *Behavior Research Methods, 45,* 880–895.

Williams, E. (1959). The comparison of regression variables. *Journal of the Royal Statistical Society, 21,* 396–399.

Xiao, X., Zhang, Q., Saleska, S., Hutyra, L., De Camargo, P., Wofsy, S., et al. (2005). Satellite-based modeling of gross primary production in a seasonally moist tropical evergreen forest. *Remote Sensing of Environment, 94,* 105–122.